scientific reports

Check for updates

OPEN

Fibration symmetries and cluster synchronization in multi-body systems

Margherita Bertè & Tommaso Gili

Structural symmetries influence synchronization patterns in complex systems. In particular, for graphs, the interplay between synchronization clusters for dynamical processes and classes of equivalent nodes with isomorphic input trees is established. Recent works generalized and proved for directed hypergraphs that balanced partitions characterize robust synchrony invariant under all admissible dynamics. In this work, we address undirected hypergraphs and identify node partitions based on equivalent incidence relations in a hypergraph, using its bipartite graph representations. We also show that, for the higher-order Kuramoto-Sakaguchi model with identical natural frequencies and identical initial conditions, fibres define invariant synchrony subspaces. Moreover, under a separating interaction-signature non-degeneracy condition, the trajectory-induced Kuramoto synchrony partition coincides with the fibration partition for almost all choices of the coupling parameters. We provide algorithms, code implementations, and visualization methods to compute local input equivalence and analyse its relation to synchronization behavior. Simulations with real-world and synthetic topologies illustrate how structural properties and representational choices affect cluster formation. We outline exploratory topology-adjustment procedures for target cluster configurations under noise and incomplete information, identifying directions for future investigations.

Keywords Fibration symmetries, Higher-order interactions, Cluster synchronization, Kuramoto model with frustration

The study of symmetry in complex systems has been central to uncovering principles governing collective dynamics, particularly synchronization. Classical approaches, grounded in group theory and graph automorphisms, have revealed how structural features shape the evolution of connected systems. Yet in many biological and technological networks, global symmetries are rare. This has led to a shift toward local symmetry frameworks, utilizing groupoid theory rather than traditional group theory. Groupoids, introduced by Brandt in 1926, have since served various mathematical contexts[1], offering a generalized framework that extends and relaxes group properties. In our context, we focus on groupoids made by graph fibration symmetries, which partition nodes based on equivalence in their input flows and have proven effective in identifying cluster synchronization patterns. Indeed, graph fibrations, a concept rooted in category theory[2], provide a useful framework to uncover synchronization patterns in complex networks and their relation with the topology[3–5]. While extensive research has focused on fibration symmetries in graphs, the growing interest in systems with higher-order interactions (HOI)[6,7] requires further development in this area. In such systems, interactions are not limited to pairs but involve groups of nodes, posing new challenges for understanding how structure governs dynamics. We position our work within this landscape by focusing on the generalization of fibration symmetries to HOI systems.

Related works

Graph fibrations and symmetry-based methods have been widely explored across different domains to understand synchronization and collective dynamics, from distributed computing[3], gene regulatory systems[8], to the neuronal network[9]. Recent advancements in network theory have shed light on the deep connection between network structure and function, particularly through the lens of graph fibrations and symmetry groups[3–5,10].

In the context of biological networks, Morone et al.[9] applied symmetry group factorization to the neural connectome of *Caenorhabditis elegans*, showing a hierarchical structure that matches broad functional categories. Further, Leifer et al.[8] applied fibration symmetries to predict synchronized gene coexpression patterns in bacterial gene regulatory networks. Their findings suggest that network structure alone can provide valuable insights into gene synchronization, potentially reflecting evolutionary pressures that have shaped gene input

IMT School for Advanced Studies, P.zza San Francesco 19, 55100 Lucca, Italy. email: margherita.berte@imtlucca.it

functions to realize coexpression. The application of these theoretical frameworks to human brain networks is beginning to yield insights into cognitive function. Makse et al.[11] applied fibration symmetry analysis to brain networks involved in language processing, revealing how symmetry breaking supports functional transitions between resting state and language engagement. That work suggests that local network symmetry in the brain may play a crucial role in determining coherent function, offering a new perspective on the structure-function relationship in neuroscience.

In all cases where global symmetries do not apply, as in the biological realm, the shift of focus from global to local patterns and their impact on the entire system has gained more attention. With this perspective, cluster synchronization refers to the phenomenon where subsets of nodes in a network synchronize their dynamics while remaining out of sync with nodes in other clusters. This behavior is often associated with structural symmetries or equitable partitions in the network, which constrain the dynamical evolution and lead to partial synchronization patterns. Different works focus on the concept of cluster (or partial) synchronization. On the one hand, providing computational perspectives through algorithms to partition the nodes[12] or to optimize the analysis of stability for local dynamical patterns[13]. On the other hand, providing a case study or a unified framework and theory related to dynamical processes and node partition[14–16].

The Kuramoto model describes coupled phase oscillators and typically leads to global synchronization under strong coupling when natural frequencies are identical. To capture more complex phenomena, such as partial or inhibited synchronization, researchers have extended the model by introducing phase-lag (frustration) terms. Nicosia et al.[17] linked these frustrated dynamics to remote synchronization mediated by network symmetries, a relationship further explored in the comprehensive overview on cluster synchronization[18]. Kirkland et al.[19] introduced α-Kuramoto partitions to study synchronization patterns constrained by a phase lag, while Brede[20] explored heterogeneous phase shifts via local frustration parameters.

Beyond pairwise interactions, higher-order interactions generalize the notion of connectivity to groups of nodes, posing additional challenges for analysing partial synchronization. Recent studies on hypergraphs or simplicial complexes often rely also on equitable partitions to understand these patterns[16,21]. Multi-body generalizations of the Kuramoto model, incorporating frustration or phase-lag parameters, have been proposed to capture more complex dynamical behaviors. However, existing generalizations have primarily focused on all-to-all configurations. Notable contributions include Dutta et al.'s asymmetric Kuramoto model for hypergraphs[22], which generalizes frustration to higher-order interactions, Moyal et al.'s work specifically addressing frustration in hypergraphs limited to three-body interactions[23], and León et al.[24], who showed that higher-order interactions with nonzero phase-lag in globally coupled ensembles can produce anomalous transitions to synchrony. Further, studies on Kuramoto models with bi and triadic interactions highlight that the impact of higher-order interactions on total synchronization can nontrivially alter both the linear and basin stability of Kuramoto dynamics[25] and that depend on the chosen representation, enhancing or suppressing collective synchronization in hypergraphs versus simplicial complexes[26]. This point aligns with recent findings by Salova et al.[27], who emphasized the impact of representational choices on synchronization dynamics.

In parallel, for multi-body interactions, the study of local symmetries has provided a structural perspective on cluster synchronization for directed hypergraphs[21,28]. In particular, Von der Gracht et al. formally extended the notion of fibrations to systems with higher-order interactions and demonstrated that balanced partitions induced by fibrations identify robust synchrony spaces for all admissible dynamics. Notably, the comprehensive work[29] about fibrations symmetries dedicates a chapter to fibrations for higher-order interactions. The scope of the present work is complementary to those results. The robust-synchrony theory characterizes partitions that are invariant for broad classes of admissible dynamics. Here, instead, we focus on a concrete dynamical system, the higher-order Kuramoto–Sakaguchi model, and study a model-specific conditional generic converse under homogeneity assumptions and a separating interaction-signature non-degeneracy condition specified below. Thus, our dynamical result should not be read as a replacement for the general admissible-dynamics characterization, but as a model-specific statement for a widely used oscillator dynamics. In particular, our objects of study are undirected hypergraphs, while for the particular case of simplicial complexes, we refer to[30], in which Nijholt et al. studied the equivalent concept of balanced coloring, considering also the orientation of the simplices. Indeed, if orientation is not considered, simplicial complexes can be regarded as a particular case of hypergraphs (with additional inclusion constraints), and the framework developed here applies. When orientation is taken into account, however, the notion of symmetry must incorporate it, leading to a different class of admissible equivalences. This setting has been studied in detail by Nijholt et al.[30], where orientation plays a central role in defining dynamical invariants. This distinction highlights that the choice of representation, and in particular whether orientation is included, directly affects both the symmetry structure and the resulting dynamics.

We also aim to prove how local structural equivalences can relate to partial synchronisation in a Kuramoto model, even between nodes that are not directly connected. This emphasizes the relevance of remote synchronization phenomena, which can arise independently of global automorphism symmetries. To this end, we focus on a nonlinear dynamical model, which allows us to capture complex behaviors that more abstract linear approaches might miss, as highlighted in[28]. We focus on fibration symmetries, as they offer a principled way to partition nodes based on identical input structures. This choice differentiates our approach from other similar studies that refer in general to symmetries or equitable partitions,[16,21]. Indeed, our notion, which corresponds to the coarsest equitable partition or minimal balanced coloring, is central to our analysis not only for its connection to dynamics but also because it captures intrinsic structural regularities that are relevant on their own. Building on the theoretical results of[21,28] for directed hypergraphs, who proved that balanced partitions characterize robust synchrony invariant under all admissible dynamics, we restrict attention to the higher-order Kuramoto model with frustration, showing first that fibre partitions define invariant synchrony subspaces and then proving a conditional generic converse: under homogeneous initial conditions, identical

natural frequencies, and a separating interaction-signature non-degeneracy condition, the trajectory-induced Kuramoto synchrony partition coincides with the fibration partition for almost all coupling parameters. Our approach intersects with the recent work[31] in the use of local symmetries and equitable relations to explain collective dynamics. While Kovalenko et al. establish general conditions for equitable synchronization in multiplex and higher-order networks, we provide computational tools and empirical validation for the specific case of higher-order Kuramoto dynamics. From a technical viewpoint, the linear independence assumptions on the coupling functions introduced in[31] play the same role as our genericity argument. In their framework, linear independence of the coupling families is imposed as a hypothesis to rule out pathological cancellations between different coupling contributions, which would allow synchrony patterns not aligned with the structurally equitable partitions. In our setting, the analogous pathological cancellations are excluded by the separating interaction-signature condition introduced below. Under this non-degeneracy condition, the remaining parameter values for which non-fibration synchrony can persist form a measure-zero subset of the parameter space.

This work refines the understanding of fibration symmetries in systems with higher-order interactions by addressing how to compute fibres in undirected hypergraphs effectively. Focusing on the higher-order Kuramoto model with frustration, a well-established setting in physics, we show that fibre partitions correspond to invariant synchronization clusters under specific structural conditions. Our analysis establishes that, starting from the agnostic case of identical oscillators with identical initial conditions, fibre synchrony is invariant, while synchrony patterns not aligned with the fibration decomposition are generically excluded under the separating interaction-signature condition, except on an exceptional parameter set. Alongside the theoretical discussion, we provide algorithmic insights and practical procedures to implement fibre detection and symmetry-preserving topology modifications. These contributions bridge abstract formulations and computational practice, offering concrete tools for analysing synchronization phenomena in complex higher-order networks. Throughout the paper, we provide visualizations and examples to illustrate key concepts, maintaining an operative perspective through algorithmic implementations and references to real-world network topologies. By integrating theoretical insights with empirical evidence, our research provides a conceptual framework and methodologies for examining HOI systems via fibration symmetries. Finally, in the concluding section, we discuss the practical challenges encountered with hypergraph fibrations in symmetry-driven network modification[32–34]. We examine hypergraph sparsification methods that preserve fibre structures while removing redundant hyperedges to reduce computational complexity and improve interpretability. Further, we investigate topology modification techniques to reconstruct hypergraph structures when observed synchronization patterns suggest that the available topology may be incomplete or corrupted due to measurement limitations or data loss.

Results

Graph fibration symmetries

This subsection introduces the formal mathematical definitions of graph fibrations. By fixing the notation and presenting common basic definitions, the aim is to provide a unified framework to facilitate the interpretation of the concepts discussed throughout this work and as a reference point for extending fibration symmetries to complex systems with higher-order interactions.

Definition 1 (*Directed graph*) A directed graph G is a tuple $G = (N, E, s, t)$ where N is the set of nodes and $E \subseteq N \times N$ is the set of edges. The source and target maps, respectively $s, t : E \to N$, associate each edge with its tail or head, namely the first or second nodes in the ordered pair of nodes constituting the edge.

Definition 2 (*Undirected graph*) An undirected graph $G = (N, E, s, t)$ is a directed graph such that $\forall e \in E$, $e = (s(e), t(e)) \Rightarrow \exists f \in E$ s.t. $f = (t(e), s(e))$.

Remark 1 An undirected graph can be characterized by specifying only the set of nodes and edges. Hence, we will omit the source and target maps.

We now proceed to define fibration symmetries for directed graphs, adopting the notation by Boldi et al.[3] who organized and presented the fibration symmetries theory for graphs.

Definition 3 Let $G = (N_G, E_G, s_G, t_G), B = (N_B, E_B, s_B, t_B)$ be directed graphs. A **graph homomorphism** $\xi : G \to B$ is given by a pair of functions $\xi_N : N_G \to N_B$ and $\xi_E : E_G \to E_B$ commuting with the source and target maps.

A **fibration** between G and B is a homomorphism $\varphi : G \to B$ such that $\forall a \in E_B, \forall x \in N_G$ satisfying $\varphi(x) = t_B(a)$ there is a unique arc $\tilde{a}^x \in E_G$ such that $\varphi(\tilde{a}^x) = a$ and $t_G(\tilde{a}^x) = x$. In literature, we refer to G as the total graph and to B as the base graph. This property is called the lifting property.

Nodes mapped in the same node in the base graph B are a **fibre**. A trivial fibre is a singleton.

Fibrations that collapse all fibres in one node in the base graph are called minimal.

Throughout the paper, we will consider in particular surjective minimal fibrations, referred to as **fibration symmetry**, following the definition in[35]. The concept of input sets and input trees, which encode the path of incoming edges to a node, was introduced by Aldis[36] and by Boldi et al.[3]. They employed these notions to prove that finding nodes having isomorphic input trees is equivalent to the existence of graph fibrations. Further, the proof of the equivalence between fibres of minimal surjective fibration and minimal balanced coloring is stated by Aldis[36]. This maximal grouping ensures that nodes are partitioned only when their input structures genuinely differ, avoiding artificial fragmentation of structurally equivalent nodes. Our approach is deliberately topology-

centric: nodes are classified by their incidence relations (i.e., by their input trees of colored input set), enabling us to isolate the role of network structure in determining synchronization.

Remark 2 Theorem II.4 can be extended to undirected graphs by treating them as bidirected graphs, meaning that each undirected edge is regarded as two directed edges that connect the two possible configurations of source and target vertices.

Makse et al.[29] provide a detailed discussion of the different notions of graph quotients that arise when one takes a node partition as an equivalence relation. The definition is subtle, since different conventions lead to different objects. In our setting, we require the quotient to coincide with the base graph in the sense of fibration symmetry. In particular, the construction must guarantee the lifting property.

Definition 4 (*Quotient graph*) Let $G = (N, E)$ be a directed graph and let $\sim$ be the equivalence relation on N induced by a fibration symmetry, i.e., $u \sim v$ whenever u and v belong to the same fibre. For $v \in N$, denote by $[v]$ the fibre containing v.

The quotient graph $G/\sim := (\bar{N}, \bar{E})$ is defined as follows:

- The node set is $\bar{N} = \{[v] \mid v \in N\}$.
- For an ordered pair of fibres $[u], [v] \in \bar{N}$, the number of directed edges between them in $\bar{E}$ equals the number of edges in G between a vertex of $[u]$ and a vertex of $[v]$.
- If u and v lie in the same fibre, loops in $\bar{E}$ record the edges of G internal to that fibre.

Thus, the quotient graph is obtained by collapsing each fibre to a single node while preserving the connectivity pattern between fibres. In Fig. 1, we depict a representation where nodes in the same fibre (with the same color) are collapsed into a unique node in the quotient graph on the right (also named base graph). We can observe that the fibration symmetry φ maps each node to a quotient node whose incoming edges originate from nodes of the same fibres as in the total graph.

Higher-order interactions

This subsection sets the notations needed to model higher-order interactions in complex systems. We recall the definitions of hypergraphs and their associated bipartite representations. We then emphasize how the incidence bipartite graph provides a natural framework for identifying fibres in multi-body interactions. Finally, we introduce the notions of fibres and fibration symmetries in the context of hypergraphs.

Definition 5 (*Directed hypergraph*) A directed hypergraph $H = (N, E)$ consists of a node set N and a set of directed hyperedges E. A directed hyperedge $e \in E$ is a pair $(T(e), H(e))$, where the tail $T(e)$ is a non-empty multiset of elements of N and the head $H(e)$ is a non-empty subset of N.

Remark 3 In our setting, we do not require an order among the nodes in the tail or head of each hyperedge, differently from[28].

As a particular case of directed hypergraphs, we can consider undirected hypergraphs (hereafter referred to as hypergraphs). They will be the focus of our work.

Definition 6 (*Hypergraph*) An undirected hypergraph $H = (N, E)$ consists of a node set N and a hyperedge set E, where each hyperedge is a non-empty multiset of nodes from N. The cardinality of a hyperedge is called its order. The rank $rk(H)$ of a hypergraph is the maximum of the orders of its hyperedges, $rk(H) = \max_{e \in E} |e|$.

Remark 4 Because hyperedges are multisets, a node may appear more than once within the same hyperedge. While this is not the standard convention in hypergraph theory, it is a natural choice when working with quotient constructions, and it has already been adopted in related contexts (e.g.[21,28]). This convention will be important here to guarantee that the quotient of a hypergraph remains a hypergraph under the current definition (refer to the hypergraph on the right in Fig. 3).

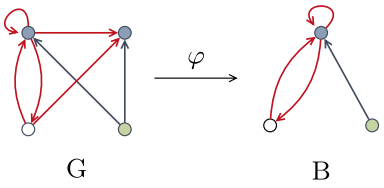


Fig. 1. Surjective graph fibration. Example of graph fibration $\varphi : G \to B$. Nodes with the same color belong to the same fibre in the total graph G and are mapped by φ to the unique node with the same color in the base graph B, which is the quotient graph.

Remark 5 An undirected hypergraph can be considered as a directed hypergraph with all possible combinations of source and target sets in each hyperedge, as nicely depicted in Figure 1 of[37].

This observation does not make the undirected setting merely redundant for our purposes. Many empirical higher-order datasets are represented and analysed directly as unordered group interactions, such as collaborations, co-participation events, or disease-gene associations. In such cases, it is useful to compute structural equivalence classes on that representation itself rather than only after translating or projecting the data, while preserving the information encoded by the undirected representation.

Remark 6 Observe that if $rk(H) = 2$, then H is an undirected graph.

Definition 7 (*Bipartite digraph*) A directed bipartite graph (or bipartite digraph) is a graph $G = (N_1 \sqcup N_2, E)$ where the nodes can be partitioned into two disjoint subsets (named layers) such that $E \subseteq N_1 \times N_2$. It means that the edges cannot contain nodes belonging to the same layer.

Incidence graph representation

A hypergraph $H = (N, E)$ can be represented via its incidence bipartite digraph $B_H = (N \sqcup E, F)$, where $F = \{(n, e) \in N \times E \mid n \in e\}$, also called factor graph[29]. In[38], the author proves a categorical equivalence between directed hypergraphs and bipartite RB-graphs. With the same perspective, in section A.1 we extend the demonstration and propose the categorical equivalence of the undirected hypergraphs and bidirectional bipartite graphs. This relationship is naturally intuitive, as the unique incidence matrix (apart from the order) of a hypergraph coincides with the unique bi-adjacency matrix of the bipartite graph having as nodes in the first layer the hypergraph nodes and as nodes in the second layer the hyperedges. Thus, a hypergraph can be handled by its incidence bipartite representation, and algorithms designed to partition graph nodes with the same input trees can be applied to hypergraph nodes by regarding them as belonging to an inhomogeneous directed graph.

Remark 7 The bipartite graph must not contain any isolated node since disconnected nodes in the second layer would represent empty hyperedges, which fall outside the formal definition of a hypergraph.

Fibration symmetries for hypergraphs

By representing the hypergraph as its incidence bipartite digraph, we can treat it as an inhomogeneous graph and thus apply fibre-computing algorithms. In this perspective, nodes corresponding to original vertices and nodes corresponding to hyperedges are explicitly distinguished from the outset by assigning them different initial types (or colors). The algorithm then partitions both sets into fibres, producing a coloring of the original nodes as well as of the hyperedges (see Fig. 2). The fibres in a hypergraph H are defined as the nodes that belong to identical fibres in the associated incidence bipartite graph B_H when B_H is treated as an inhomogeneous graph. Fibration symmetries for HOI are fibrations symmetries for the inhomogeneous graph representation of the incidence bipartite graph of the hypergraph, preserving the colors of the original nodes and hyperedges.

For hypergraphs, the quotient construction is performed on the incidence bipartite graph, and the resulting quotient can then be translated back into the hypergraph setting. A key point is that preserving multi-body interactions may require allowing repeated occurrences of quotient nodes within the same hyperedge. Figure 3 illustrates a fibration symmetry on a hypergraph. Nodes on the left are mapped to nodes of the same shape and color on the right. In the quotient on the right, some nodes appear multiple times in a single hyperedge, highlighting the role of multisets in the definition of a hypergraph. It is also worth noting that, as for quotient in graphs, even if the original hypergraph is undirected, its quotient need not be. Indeed, when two distinct nodes

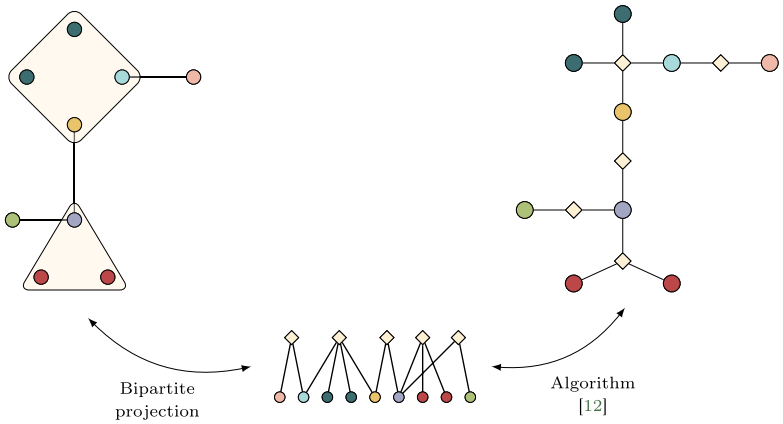


Fig. 2. Workflow to find fibres in hypergraphs. Starting from an undirected hypergraph, we can associate its incidence bipartite projection. Considering it as an inhomogeneous graph, we can apply standard graph algorithms, as the version of[12] revised by[39], to obtain the hypergraph node partition, here depicted with different colors.

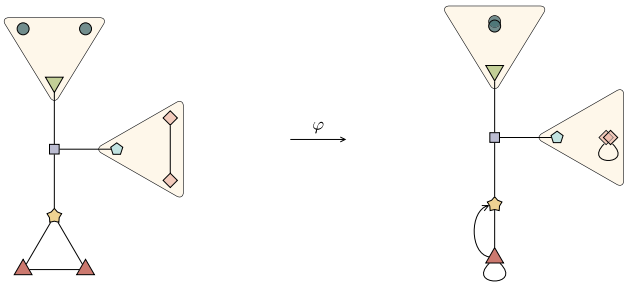


Fig. 3. Hypergraph quotient via fibration symmetry. The left hypergraph shows the original structure where nodes with identical shapes and colors represent distinct vertices belonging to the same fibre under the fibration map φ (i.e., nodes receiving equivalent input information). The right side depicts the quotient hypergraph, where nodes with matching shapes and colors represent a single supernode corresponding to an entire fibre. In the quotient representation, slightly overlapping identical nodes within hyperedges indicate multiple instances of the same supernode participating in that hyperedge, preserving the structural information while reducing redundancy through the fibration symmetry φ. Edges without arrows are undirected (equivalent to having arrows in both directions).

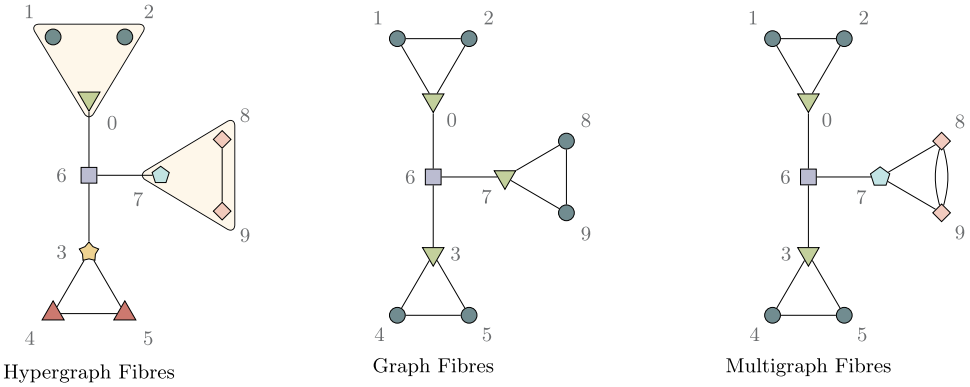


Fig. 4. Different fibre partitions according to the chosen representation. Example of fibres for a hypergraph, its projection to a simple graph, and its projections to a graph with multiple edges. In each representation, nodes belonging to the same fibres are pictured with the same color and icon.

of the same fibre are connected to a common node in the original hypergraph, collapsing them in the quotient may introduce a non-reciprocated edge, thereby breaking undirectedness.

Remark 8 Observe that different types of node partitioning can emerge depending on whether we analyse a hypergraph, its binary graph projection, or its multigraph projection. Each representation captures different structural features of the original hypergraph. The binary graph projection simplifies the hypergraph by representing only the existence of pairwise interactions, discarding information about the number or order of interactions. As a result, it overlooks distinctions between higher-order relationships and repeated interactions, leading to a fibre structure that lacks key information. In contrast, the multigraph projection preserves the multiplicity of interactions between pairs of nodes, capturing how frequently node pairs co-occur in hyperedges. However, it still treats all interactions as equivalent, regardless of their order, thus failing to distinguish the structural role of higher-order interactions.

This behavior is illustrated with an example in Fig. 4. The left panel shows a hypergraph, where nodes are grouped into fibres based on their participation in higher-order hyperedges (represented by shaded regions). In the middle panel, the binary graph projection loses both the frequency and the order of these interactions, resulting in a different, less informative fibre structure. The right panel, representing the multigraph projection, captures repeated pairwise connections but still ignores the original hyperedge order, leading to distinct partitioning.

Algorithm

In section "Higher-order interactions", we discussed how, thanks to the equivalence of a hypergraph and its bipartite projection, we can utilize established algorithms, such as those presented in[12]. In this section, we report an algorithm to obtain the partition of the nodes of an input hypergraph according to the fibres. The following Algorithm 1 proceeds by projecting the hypergraph into its bipartite representation and then applying

an iterative color refinement scheme. The notation and the steps follow the algorithm presented in[39]. Hence, the complexity to assign colors to nodes and hyperedges of a hypergraph $H = (N, E)$ scales as $O(|F| \, log(|N| + |E|))$, where F is the set of edges in the bipartite representation of H.

For clarity, we present the simplified formulation in Algorithm 1, whereas the full, extended version is provided in Algorithm 3 within the Supplementary Material.

Remark 9 The algorithm of Morone et al.[39] may fail only in the rare presence of multiple disconnected components or distinct nodes without inputs, as shown in counterexample 7.3 of[35]. In our case, this failure does not occur, since we only consider the undirected case with a single connected component. Moreover, as implemented in our algorithm (see section "Code availability"), the initial color dictionary is provided as input to distinguish between original nodes and hyperedges, so assigning distinct initial colors to source nodes would, in any case, prevent such ambiguity.

Input: Hypergraph $H = (N, E)$.
Output: Fibre partition of nodes and hyperedges.
Construct the incidence bipartite graph $B_H = (N \sqcup E, F)$, where $F = \{(n, e) \in N \times E \mid n \in e\}$.
Assign one initial color to hypergraph nodes and another to hyperedges.
Repeat:

- for each vertex of B_H, count the colors appearing in its input set;
- update its color according to this input-color profile;

until the coloring stabilizes.
Return the final colors on N and on E.

Algorithm 1. Simplified workflow for finding fibres in a hypergraph.

Exploratory topology modifications

Beyond computing fibres, the incidence-fibration framework can also be used to formulate topology-modification tasks. In section A 3, we describe three exploratory heuristic procedures: fibre-preserving sparsification, topology correction toward a prescribed fibre partition, and redundancy injection preserving a prescribed partition. These algorithms are intended as constructive prototypes rather than optimized or benchmarked methods. They illustrate how fibre information can constrain hypergraph modification, while systematic evaluation of optimality, scalability, and comparison with graph-based methods is left for future work.

Fibration symmetries for real-world datasets with HOI

To illustrate the relevance of fibration symmetries beyond theoretical models, we analyse several real-world systems featuring higher-order interactions. We computed the nodes partition via fibration symmetry for some datasets with higher-order interactions provided by XGI dataset[40]. In addition, we calculated the fibres for an emblematic example of higher-order interactions in real-world situations: collaborations among researchers for publishing a paper in a conference. We considered the MAG-10 dataset[41,42], preprocessed in https://github.com/TheoryInPractice/overlapping-ecc/tree/master/data/MAG-10, a subset of the Microsoft Academic Graph in which the nodes are the authors (labelled with a code), the hyperedges correspond to a publication by those authors, and the hyperedges are categorised according to one of the 10 computer science conferences, the most common conference in which they published. In particular, we considered the *International Conference on Machine Learning* (ICML), filtering by code 3, the *International World Wide Web Conference* (WWW), filtering by code 2, and the *International Conference on Computer Vision* (ICCV) with code 8. In this dataset, articles with more than 25 authors are omitted (Table 1).

As observed in Theorem II.15, for the MAG-10 dataset related to the ICML conference, representing paper collaborations through a hypergraph rather than a multigraph alters the fibres. The case depicted in Fig. 5 illustrates how, in the multi-edge projection, the two authors with codes 7979 and 4508 are placed in the same fibre, despite having collaborated in different ways with the same authors (with codes 4509, 7980). Indeed, while the author 7979 collaborated on one paper with the other two authors 4509, 7980 together, the author 4508 produced two papers in two different collaborations with each of the individual authors. The graph representation with multiple edges flattens this case by not recognizing the different types of collaboration by bringing them together. An analogue mismatch occurs for the dataset corresponding to the publication in the International World Wide Web Conference. Specifically, at WWW, the author identified as 21331 co-authored two separate papers with authors 21332 and 22750, while the author with code 32176 collaborated with both on a single paper. In the multigraph representation, a fibre includes authors 32176 and 21331, failing to differentiate their distinct publishing contributions. The same situation occurs for the two pairs of authors with code 18628, 51267 and 2149, 37684 related to ICCV.

Cluster synchronization

Having established the structural foundations through definitions and illustrative examples of fibrations for higher-order interactions, we now turn to the dynamical aspects of the system. To ensure compatibility between

Dataset	|N|	|E|	|N|/|C|	# Non-trivial fibres
diseasome	516	314	1.46	94
disgenenet	12368	1672	1.39	629
hospital-lyon	75	1824	1.00	0
house-committees	1290	335	1.07	51
hypertext-conference	113	2434	1.00	0
invs13	92	787	1.00	0
MAG-10 (ICML)	9981	4803	2.32	1354
MAG-10 (WWW)	12889	5468	2.42	1829
MAG-10 (ICCV)	11693	5367	2.30	1683
malawi-village	84	431	1.01	1
ndc-classes	628	796	1.51	165
ndc-substances	3414	6471	1.16	248
plant-pollinator-mpl-015	130	401	1.02	2
plant-pollinator-mpl-016	26	73	1.04	1
plant-pollinator-mpl-049	37	91	1.00	0
plant-pollinator-mpl-062	456	866	1.00	0
science-gallery	410	3350	1.00	1

Table 1. Summary table showing the nodes partition in fibres across different datasets with HOI. The table reports for each dataset, the number of nodes $|N|$, the number of edges $|E|$ excluding singletons. Considering $|C|$ as the number of fibres partitioning the nodes via higher-order symmetry fibrations, we report the average number of nodes in each fibre $|N|/|C|$ and, in the last column, the number of nontrivial fibres, all the fibres formed by more than one node.

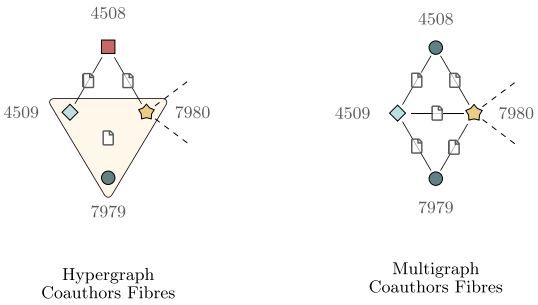


Fig. 5. Visualization of different fibre partitions based on the representation of the co-author relationship. Example of different fibres between the hypergraph representation and its multigraph projection in a real-world case for collaboration on publications for the ICML conference (MAG-10 dataset filtered for ICML conference). Nodes represent authors, and paper collaborations are depicted with a hyperedge among the authors, stressed with a paper icon. Nodes painted with the same color and mark belong to the same fibre. For the sake of the example, in this image, we represent only the papers related to authors labeled with codes 7979 and 4508. Nodes 4509 and 7980 are in different fibres in both cases as they are related (illustrated with dashed lines) to different other nodes not present in the picture.

the dynamics and the underlying hypergraph structure, we consider admissible ODE systems[21,28], where the evolution of each node depends only on the structure-prescribed interactions. The higher-order Kuramoto model with frustration (Kuramoto-Sakaguchi) falls within this class, as its dynamics respect the hypergraph topology and involve only interactions explicitly defined by the system's combinatorial structure. In this section, we introduce the dynamical model and examine how the underlying structural features influence its behavior. We aim to connect the structural characterization of robust synchrony due to Von der Gracht et al. and Aguiar et al. with the behavior of the higher-order Kuramoto dynamics, showing in particular that synchrony in this model with homogeneous initial conditions and natural frequencies is constrained to the fibration partition, under the assumptions below.

Higher-order Kuramoto model with phase-lag parameters

We study synchronization dynamics in oscillator populations using a Kuramoto model with both pairwise and three-body interactions. Although our framework refers broadly to higher-order interactions, we focus on two- and three-body terms as the minimal setting that captures collective behaviors beyond standard pairwise coupling. Our primary interest lies in cluster and remote synchronization, where phase alignment of identical

oscillators occurs only within specific groups of nodes, rather than across the entire network. The inclusion of three-body interactions follows the principled derivation of León et al.[24], who used phase reduction techniques to show that such interactions naturally arise in the form $\sin(\theta_\gamma + \theta_\delta - 2\theta_a - \alpha)$ for an oscillator a. While León et al.'s formulation assumes all-to-all coupling, we generalize it to arbitrary network topologies, in line with Muolo et al.[43]. Crucially, we retain the phase-lag parameter, which makes the coupling non-invasive no longer at the fully synchronous state and allows input-profile differences to affect the vector field, enabling the network to exhibit nontrivial collective states, even with identical oscillators starting with identical initial conditions.

Model Consider a hypergraph $H = (N, E)$, with rank $rk(H) \leq 3$. Define the incidence matrix of order m with $m \in \{2, 3\}$ as the matrix $I^{(m)}$ with as many rows as the cardinality of N and as many columns as the cardinality of $\mathcal{E}^{(m)} = \{e \in E \mid |e| = m\}$, that is the set of hyperedges of order m. Then $\forall i \in N, e \in E$:

$$[I^{(m)}]_{i,e} = \begin{cases} 1 & \text{if } i \in e \\ 0 & \text{otherwise} \end{cases}$$

The evolution of each node $i \in N$ can be expressed as follows:

$$\dot{\theta}_i = \omega_i + \sum_{m=2}^{3} \sigma_m \sum_{e \in \mathcal{E}^{(m)}} [I^{(m)}]_{i,e} \sin\Big(\sum_{j \in e \setminus \{i\}} \theta_j - (m-1)\theta_i - \alpha^{(m)} \Big), \tag{1}$$

where σ_m is the strength of the mth order coupling and ω_i is the natural frequency of the oscillator associated with the node. Angles $\alpha^{(m)} \in (0, \pi/2)$ are the phase frustration parameters for each order m. With nonzero frustration, the coupling no longer vanishes at the fully synchronous state, so input-profile mismatches can affect the vector field; full synchrony is not generically invariant unless the relevant weighted input profiles match. To isolate the role of the network structure and frustration in shaping these patterns, we will assign identical initial conditions and natural frequencies to all nodes. This choice reflects an anonymity condition in the sense of[29], ensuring that any observed symmetry breaking arises purely from the dynamics and topology, rather than from imposed heterogeneity.

Remark 10 We observe that the coupling function of the Kuramoto model for identical oscillators with phase-lags $\alpha^{(m)} = 0$ for all m is non-invasive (i.e., evaluated in $\theta_i = \theta^*$ for all i is identically 0). Hence, a solution exists for global system synchronization. By inserting non-zero $\alpha^{(m)}$ instead, we avoid this case.

Synchronization measures A common way to measure coherence among a subset of nodes evolving according to a Kuramoto model is to compute the Kuramoto order parameters. We will compare global and cluster order parameters to analyse their evolution in time.

Definition 8 (*Kuramoto Order parameters*) The global Kuramoto order parameter for oscillators associated to nodes in a hypergraph $H = (N, E)$ is defined as

$$R(t) = \left| \frac{1}{|N|} \sum_{j \in N} e^{i\theta_j(t)} \right|$$

where $R(t) \in [0, 1]$ quantifies the overall phase coherence of the system. Given a cluster $C_\alpha \subseteq N$, the local order parameter is

$$R_\alpha(t) = \left| \frac{1}{|C_\alpha|} \sum_{j \in C_\alpha} e^{i\theta_j(t)} \right|$$

where $R_\alpha(t) \in [0, 1]$ measures the synchronization within cluster C_α.
The Kuramoto order parameter is a measure of phase coherence among a group of oscillators. It takes values between 0 and 1, where 1 indicates perfect synchronization, all nodes are in phase, while values closer to 0 reflect increasing incoherence.

Figures 6 and 7 present the temporal evolution of global and local order parameters for fibre configurations across two hypergraph architectures: synthetic networks, and the diseasome. In all the images, we can see that at $t = 0$ all the parameters are 1, as the initial conditions are set equal for all nodes. During the evolution, local order parameters for fibre clusters remain constant at unity across all hypergraph types, while global order parameters exhibit deviations from unity. This divergence indicates that global coherence breaks down despite the preservation of local cluster organization, indicating the influence of network topology on these dynamics.

To assess whether this fibre-based coherence remains informative beyond the exactly homogeneous setting, we also performed a finite-time weak-heterogeneity check in section A 2. We perturbed either the initial phases or the natural frequencies by independent Gaussian perturbations and measured the resulting fibre-cluster coherence. The results, reported in Figure 10, show that the fibre order parameters remain close to one for weak heterogeneity and degrade progressively as the perturbation amplitude increases. This analysis is intended as a numerical robustness diagnostic and not as a stability result.

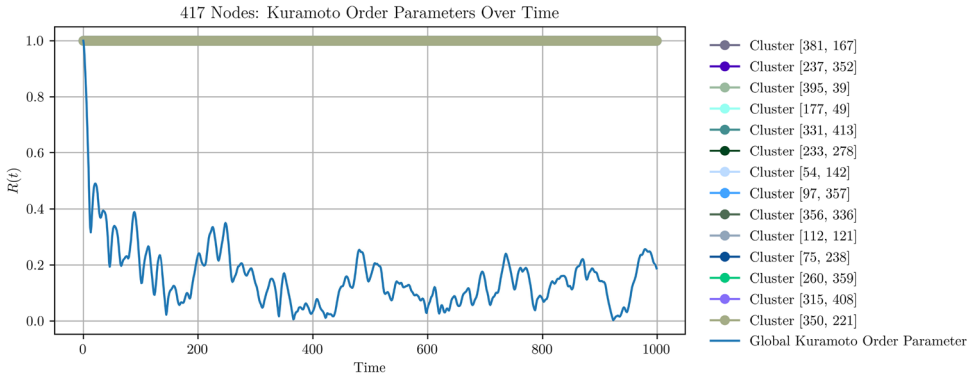


Fig. 6. Cohesiveness measure in fibres and globally for a synthetic hypergraph. The Kuramoto order parameters R for different fibres and for the whole hypergraph for a higher-order Kuramoto model with frustration (Eq. (1) with $|N| = 417$, $\alpha = \pi/6$ and $(\sigma_2, \sigma_3) = (0.2, 0.6)$). When R is closer to 1, the phases of all nodes are more synchronized. The local order parameters for all fibres overlap and are identically 1. The blue thin line is the global order parameter.

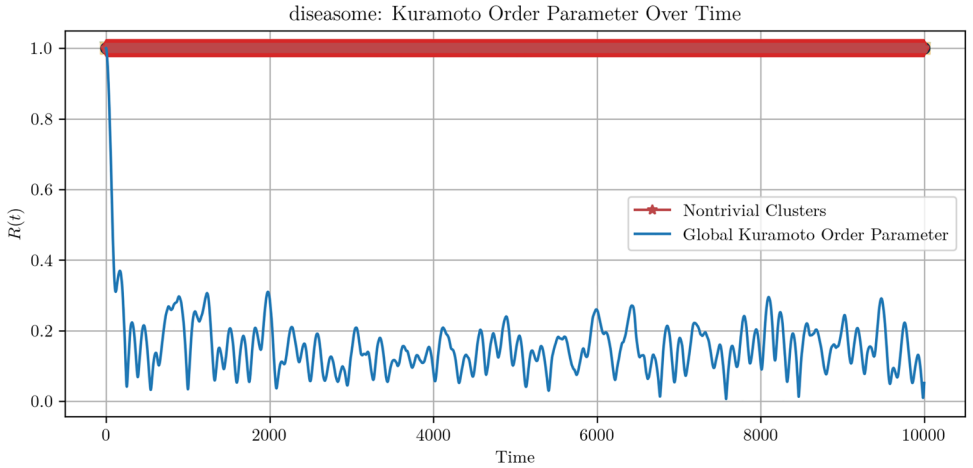


Fig. 7. Cohesiveness measure in fibres and globally for the diseasome dataset. The Kuramoto order parameters R for the nontrivial fibres and for the whole hypergraph with a higher-order Kuramoto model with frustration (Eq. (2), with $\alpha = \pi/6$). The topology is from the largest connected component without duplicate edges of the *diseasome* dataset (94 nontrivial clusters)[44]. In this dataset, a disease is a node, and a gene is a hyperedge. When R is closer to 1, the phases of all nodes are more synchronized. In red, the overlapped fibre order parameters are identically equal to 1 for all 94 non-trivial fibres.

Fibration and Kuramoto synchrony partitions in the Kuramoto model

We now analyse the relations between the nodes' partition of a hypergraph in fibres and a Kuramoto synchrony partition starting from identical initial conditions and natural frequencies for all nodes. We first recall that the implication *fibration partition* ⇒ *Kuramoto synchrony partition* (Theorem 3.4) follows directly from the general theory[21] as the vector field associated with our model is admissible. We include a proof in the specific Kuramoto setting for completeness. More precisely, this implication shows that the fibre relations define an invariant synchrony subspace: nodes in the same fibre remain synchronized under the homogeneous dynamics. The second implication proven in Theorem 3.8 addresses the converse direction under the separating interaction-signature condition stated below: in our restricted Kuramoto framework with homogeneous initial conditions and natural frequencies, the trajectory-induced Kuramoto synchrony partition coincides with the fibration partition for almost every choice of parameters satisfying this non-degeneracy condition. To introduce the notion of a subspace of the hypernetwork's total phase space characterized by the equality of node phases, we define a Kuramoto synchrony partition of the nodes according to their trajectories. We generalize the definition of α-Kuramoto partition[19] to emphasize the dynamical nature of these partitions in the context of the Kuramoto model with frustration.

Definition 9 (*Kuramoto synchrony partition*) Given an undirected hypergraph $H = (N, E)$ with rank $rk(H) \leq 3$, take a set of 2 parameters $\{\alpha^{(m)}\}_{m\in\{2,3\}}$ with every $\alpha^{(m)} \in (0, \pi/2)$. Consider the trajectories θ_i for the nodes resulting from the Eq. (1) with parameters $\{\alpha^{(m)}\}_m$, $\sigma_2, \sigma_3 > 0$ identical natural frequencies $\omega_i = \omega$ and in-

itial conditions $\theta_i(0) = \theta_i^0, \quad i \in N$ for all nodes. We call Kuramoto synchrony partition the node partition $N = S_1 \sqcup \cdots \sqcup S_h$ such that:

- $i, j \in S_a$ if $\theta_i(t) = \theta_j(t)\ \forall t \geq 0$.
- if $i \in S_a$ and $\ell \in S_b$ with $a \neq b$, then there exists some $t \geq 0$ such that $\theta_i(t) \neq \theta_\ell(t)$.

In a nutshell, nodes with the same trajectories throughout the process are in the same cluster, while nodes with different trajectories must be in different clusters. Observe that belonging to the same cluster results in the same trajectory for all t, which we can indicate with the cluster index $\theta_i(t) = \theta_a(t)$ for all nodes i in cluster S_a. We can reduce the number of frustration parameters to just one α angle belonging to $(0, \pi/2)$, as non-zero frustration prevents the coupling from being non-invasive at full synchrony and helps expose input-profile mismatches. As we can see in the example in Fig. 8, the chosen non-null frustration parameters break global phase coherence for that topology and parameter range. Hence, for simplicity, for all m, we can set $\alpha^{(m)} = \alpha$.

We can also restate the evolution for a node i in the cluster S_a of the Kuramoto synchrony partition (Eq. (1)), emphasizing the node's membership in a cluster.

$$\dot{\theta}_i = \omega_i + \sigma_2 \sum_{\beta=1}^{h} k_{i\beta}^{(2)} \sin\left(\theta_\beta - \theta_a - \alpha\right) + \sigma_3 \sum_{\gamma=1}^{h} \sum_{\delta=\gamma}^{h} k_{i\gamma\delta}^{(3)} \sin\left(\theta_\gamma + \theta_\delta - 2\theta_a - \alpha\right). \tag{2}$$

where the double sum with $\delta \geq \gamma$ avoids double-counting symmetric pairs of clusters in three-body interactions, after fixing an arbitrary ordering of the clusters $\{S_1, \ldots, S_h\}$. We denote $k_{i\gamma_1 \cdots \gamma_{m-1}}^{(m)}$ as the number of nodes sharing a hyperedge of order m with node i and belonging to the clusters specified by the remaining $m-1$ indices of k. It can be considered as the degree of the node i of order m linking i to the different subsets of clusters. We can prove the first implication by generalizing the proof of[19]. This theorem can also be simply derived from the general theory of[21].

Theorem 1 (Fibration partition ⇒ invariant Kuramoto synchrony subspace) *Let $H = (N, E)$ be a connected hypergraph with rank at most 3. Consider the fibration-partition $\{C_1, \ldots, C_h\}$ of the nodes given by the fibres of the hypergraph. Then for any $\alpha \in (0, \pi/2)$, $\sigma_2, \sigma_3 > 0$, nodes in the same fibre remain synchronized for all time under identical natural frequencies and identical initial conditions.*

Proof Consider a system of equations associated with the fibres C_a for $a \in \{1, \ldots, h\}$ with initial conditions $x_a(0) = x_0$ and natural frequency ω:

$$\dot{x}_a = \omega + \sigma_2 \sum_{\beta=1}^{h} k_{a\beta}^{(2)} \sin\left(x_\beta - x_a - \alpha\right) + \sigma_3 \sum_{\gamma=1}^{h} \sum_{\delta=\gamma}^{h} k_{a\gamma\delta}^{(3)} \sin\left(x_\gamma + x_\delta - 2x_a - \alpha\right).$$

We denote with $k_{a\beta}^{(2)}$ (resp. $k_{a\gamma\delta}^{(3)}$) the number of hyperedges of order 2 (resp. 3) shared by nodes in fibre C_a and C_b (resp. C_a, C_γ and C_δ). By the property of the fibration partition, all nodes $i, j \in C_a$ have the same incidence

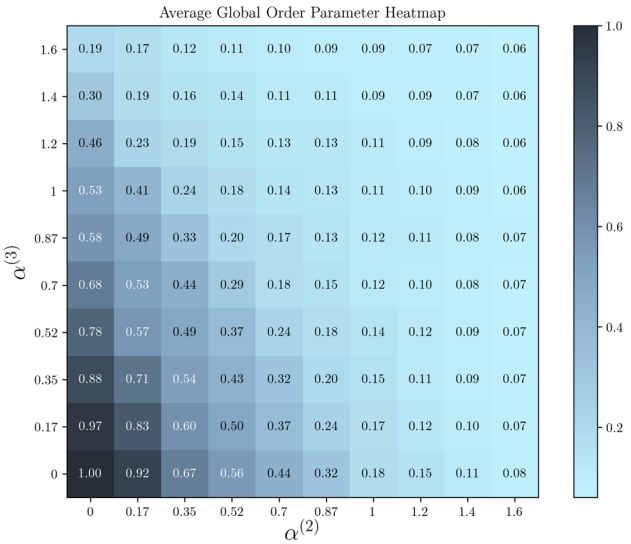


Fig. 8. Global order parameters through varying coupling force parameter options. The average global order parameter $\langle R(t) \rangle_t$ computed over 500 time steps when changing the frustration parameters of Eq. (1) with $\alpha_2, \alpha_3 \in [0, \pi/2)$. When $\langle R(t) \rangle_t$ approaches 1, it indicates near-complete phase alignment across all nodes.

counts toward the fibres: $k^{(2)}_{i\beta} = k^{(2)}_{j\beta}$ for all β, and $k^{(3)}_{i\gamma\delta} = k^{(3)}_{j\gamma\delta}$ for all $\gamma \leq \delta$. This justifies the notation $k^{(2)}_{a\beta}$ and $k^{(3)}_{a\gamma\delta}$ for the common values. Since the evolution equation has continuous partial derivatives with respect to every x_a, by Picard's theorem of existence and uniqueness of the Cauchy problem, every differential equation has a unique solution associated with the initial condition. Now consider the system of $|N|$ Equation (1). Set the same initial condition and natural frequencies for each node in the hypergraph $(\theta_i(0), \omega_i) = (x_0, \omega)$. For each node $i \in C_a$, we consider the equation:

$$\dot{\theta}_i = \omega + \sigma_2 \sum_{\beta=1}^{h} k^{(2)}_{i\beta} \sin\left(\theta_\beta - \theta_a - \alpha\right) + \sigma_3 \sum_{\gamma=1}^{h} \sum_{\delta=\gamma}^{h} k^{(3)}_{i\gamma\delta} \sin\left(\theta_\gamma + \theta_\delta - 2\theta_a - \alpha\right)$$

The same uniqueness argument applies here. All nodes $i \in C_a$ share the coefficients $k^{(m)}_{a,\beta}$ and thus satisfy the same ODE. Therefore, $\theta_i(t) = x_a(t)$ is the unique solution for each $a \in \{1, \dots h\}$, for all $i \in C_a$ and $t \geq 0$, i.e., all nodes in the same fibre evolve identically. □

Remark 11 When we assign identical initial conditions to all nodes, we eliminate the case of more refined equitable partitions (EP). This is because in finer partitions, nodes that share the same input tree structure could end up in separate clusters created by the EP if the natural frequencies or the initial conditions are different. However, since these nodes follow identical evolution equations and start with the same initial conditions, they would naturally belong to the same cluster under the Kuramoto synchrony partition. This means that nodes artificially separated into different clusters would still synchronize with each other. Our objective is to identify the largest possible clusters where all nodes within each cluster achieve synchronization. Therefore, identical initial conditions prevent the trajectory-induced synchrony partition from splitting a fibre. The reverse question, namely whether different fibres can nevertheless have identical trajectories, is precisely the generic converse addressed below and requires the separating non-degeneracy assumption.

Remark 12 Observe first that nodes in the same cluster for the Kuramoto synchrony partition must satisfy a parameter-independent first-order degree condition. Indeed, let $S_1 \sqcup \cdots \sqcup S_j = N$ be the Kuramoto synchrony partition. Let i and j belong to the same cluster; by definition, they have the same trajectory and hence the same ODE for all $t \geq 0$. We indicate with $k^{(m)}_i$ the generalized degree of order m for node i, i.e. the number of hyperedges of order m containing the node i. Their difference equation at $t = 0$ is the following:

$$\dot{\theta}_i(0) - \dot{\theta}_j(0) = -\sin\alpha \sum_{m=2}^{3} \sigma_m (k^{(m)}_i - k^{(m)}_j) = 0.$$

Starting from the same initial conditions and natural frequencies for all nodes in the hypergraph, the only way to obtain $\dot{\theta}_i(0) = \dot{\theta}_j(0)$ for all pairs of nodes $i, j \in S_a$ and independently of the $\{\sigma_m\}_m$, is to have the same degree sequence, as the frustration parameter belongs to the interval $(0, \pi/2)$. Namely:

$$k^{(m)}_i = k^{(m)}_j \quad \forall m, \forall i, j \in S_a.$$

Kirkland et al. in[19] prove that all equitable partitions in graphs are Kuramoto synchrony partitions (called α -Kuramoto partitions). However, the reverse does not always hold in their setting. Starting from initial conditions that differ for each partition, graphs can exhibit synchronization among nodes with specific degree relations, even if they do not belong to the same cluster of the equitable partition. How does this extend to hypergraphs where nodes share identical initial conditions and natural frequencies? We now state a conditional generic converse. The forward implication from fibres to synchrony is structural in the homogeneous setting. The reverse implication requires an additional non-degeneracy condition excluding exact cancellations among the interaction signatures available to the chosen dynamics. Under this condition, non-fibration synchrony can occur only on an exceptional parameter set.
Using the cluster representation θ_β for the common phase of all nodes in cluster S_β, we can write for all $i, j \in S_a$:

$$\dot{\theta}_i = \omega_0 + \sigma_2 \sum_{\beta=1}^{h} k^{(2)}_{i\beta} \sin\left(\theta_\beta - \theta_a - \alpha\right) + \sigma_3 \sum_{\gamma=1}^{h} \sum_{\delta=\gamma}^{h} k^{(3)}_{i\gamma\delta} \sin\left(\theta_\gamma + \theta_\delta - 2\theta_a - \alpha\right)$$

$$\dot{\theta}_j = \omega_0 + \sigma_2 \sum_{\beta=1}^{h} k^{(2)}_{j\beta} \sin\left(\theta_\beta - \theta_a - \alpha\right) + \sigma_3 \sum_{\gamma=1}^{h} \sum_{\delta=\gamma}^{h} k^{(3)}_{j\gamma\delta} \sin\left(\theta_\gamma + \theta_\delta - 2\theta_a - \alpha\right).$$

where the double sum with $\delta \geq \gamma$ avoids double-counting three-body interactions, after fixing an order for the clusters $\{S_1, \dots, S_h\}$. For ease of notation, we omit the dependence of θ on t. The difference $\dot{\theta}_i - \dot{\theta}_j$ can be written as:

$$\dot{\theta}_i - \dot{\theta}_j = \sigma_2 \sum_{\beta=1}^{h} (k^{(2)}_{i\beta} - k^{(2)}_{j\beta}) \sin\left(\theta_\beta - \theta_a - \alpha\right) + \sigma_3 \sum_{\gamma=1}^{h} \sum_{\delta=\gamma}^{h} (k^{(3)}_{i\gamma\delta} - k^{(3)}_{j\gamma\delta}) \sin\left(\theta_\gamma + \theta_\delta - 2\theta_a - \alpha\right) \tag{3}$$

Separating interaction signatures. For the converse direction, we impose a non-degeneracy condition on the interaction signatures available to the Kuramoto–Sakaguchi dynamics. We restrict to positive coupling strengths and define the parameter domain $\Omega = (0, \pi/2) \times (0, \infty)^2$, with $p = (\alpha, \sigma_2, \sigma_3)$. Fix a candidate node partition $S = \{S_1, \dots, S_h\}$ of N. For each block S_a, choose a representative node $r_a \in S_a$. We define the representative reduced dynamics associated with S by

$$\dot{x}_a = \omega_0 + \sigma_2 \sum_{\beta=1}^{h} k^{(2)}_{r_a\beta} \sin(x_\beta - x_a - \alpha) + \sigma_3 \sum_{\gamma=1}^{h} \sum_{\delta=\gamma}^{h} k^{(3)}_{r_a\gamma\delta} \sin(x_\gamma + x_\delta - 2x_a - \alpha),$$

with identical initial conditions $x_a(0) = \theta_0$, for all $a = 1, \dots, h$. Here $k^{(2)}_{r_a\beta}$ and $k^{(3)}_{r_a\gamma\delta}$ denote the pairwise and three-body incidence counts of the representative node r_a toward the blocks of the candidate partition S, with the same convention used in Eq. (2). This reduced system is defined for every $p \in \Omega$, independently of whether S is an actual Kuramoto synchrony partition of the full system. Since the vector field is analytic, its solution, denoted by $x^S(t; p)$, depends real-analytically on t and p locally in time. In particular, for every fixed finite time t_0, the quantities defined below are real-analytic functions of $p \in \Omega$. For a receiving block S_a, define the pairwise signatures

$$s^{(2),S}_{a\beta}(t; p) = \sin\big(x^S_\beta(t; p) - x^S_a(t; p) - \alpha\big),$$

and the three-body signatures

$$s^{(3),S}_{a\gamma\delta}(t; p) = \sin\big(x^S_\gamma(t; p) + x^S_\delta(t; p) - 2x^S_a(t; p) - \alpha\big), \qquad \gamma \le \delta.$$

We say that the interaction signatures are separating if, for every candidate partition S, every choice of representatives $\{r_a\}_{a=1}^h$, every receiving block S_a, and every nonzero family of integer coefficients $c^{(2)}_\beta$ and $c^{(3)}_{\gamma\delta}$ that can arise as incidence-count differences, with respect to the blocks of S, between two nodes in S_a, the function

$$G^S_{a,c}(t; p) = \sigma_2 \sum_{\beta=1}^{h} c^{(2)}_\beta s^{(2),S}_{a\beta}(t; p) + \sigma_3 \sum_{\gamma=1}^{h} \sum_{\delta=\gamma}^{h} c^{(3)}_{\gamma\delta} s^{(3),S}_{a\gamma\delta}(t; p)$$

is not identically zero as a real-analytic function of (t, p). Equivalently, for every such nonzero incidence-count difference vector c, there exist a finite time $t_0 \ge 0$ and a parameter value $p_0 \in \Omega$ such that $G^S_{a,c}(t_0; p_0) \neq 0$. Thus, along any representative reduced dynamics associated with a candidate partition, the pairwise and three-body interaction signatures admit no nontrivial integer linear relation, compatible with incidence-count differences, that vanishes identically.

Lemma 1 *Let $H = (N, E)$ be a connected hypergraph with* $\mathrm{rk}(H) \le 3$, *and consider the dynamics of Eq.* (1) *with identical natural frequencies and identical initial conditions. Assume the separating interaction-signature condition stated above. Then, for almost every $p = (\alpha, \sigma_2, \sigma_3) \in \Omega$, every Kuramoto synchrony partition is equitable with respect to the interaction structure read by the dynamics. More explicitly, if i, j belong to the same synchrony block S_a, then*

$$k^{(2)}_{i\beta} = k^{(2)}_{j\beta} \text{ for all } \beta, \qquad k^{(3)}_{i\gamma\delta} = k^{(3)}_{j\gamma\delta} \text{ for all } \gamma \le \delta.$$

Proof Fix a candidate partition $S = \{S_1, \dots, S_h\}$ of N, and suppose that, for some parameter value $p^* \in \Omega$, S is a Kuramoto synchrony partition. Take two nodes $i, j \in S_a$. By the definition of Kuramoto synchrony, $\theta_i(t; p^*) = \theta_j(t; p^*)$ for all $t \ge 0$, and therefore $\dot{\theta}_i(t; p^*) - \dot{\theta}_j(t; p^*) \equiv 0$. Choose one representative $r_b \in S_b$ for each block S_b. Since S is a synchrony partition at p^*, the common block trajectory coincides, by uniqueness of solutions, with the solution of the representative reduced system associated with S at p^*. Hence, for all $b = 1, \dots, h$,

$$x^S_b(t; p^*) = \theta_\ell(t; p^*) \qquad \text{for every } \ell \in S_b.$$

Using the phase-difference equation, the identity $\dot{\theta}_i(t; p^*) - \dot{\theta}_j(t; p^*) \equiv 0$ can therefore be written as

$$0 = \sigma_2 \sum_{\beta=1}^{h} \left(k^{(2)}_{i\beta} - k^{(2)}_{j\beta}\right) s^{(2),S}_{a\beta}(t; p^*) + \sigma_3 \sum_{\gamma=1}^{h} \sum_{\delta=\gamma}^{h} \left(k^{(3)}_{i\gamma\delta} - k^{(3)}_{j\gamma\delta}\right) s^{(3),S}_{a\gamma\delta}(t; p^*).$$

Equivalently, $G^S_{a,c}(t; p^*) \equiv 0$, where $c^{(2)}_\beta = k^{(2)}_{i\beta} - k^{(2)}_{j\beta}$, and $c^{(3)}_{\gamma\delta} = k^{(3)}_{i\gamma\delta} - k^{(3)}_{j\gamma\delta}$. Assume, by contradiction, that at least one of these incidence-count differences is nonzero. Then $c \neq 0$. By the separating interaction-signature condition, there exist a finite time $t_0 \ge 0$ and a parameter value $p_0 \in \Omega$ such that $G^S_{a,c}(t_0; p_0) \neq 0$. Therefore the map

$$F^S_{a,c,t_0} : \Omega \to \mathbb{R}, \qquad F^S_{a,c,t_0}(p) = G^S_{a,c}(t_0; p),$$

is a real-analytic function on the connected open domain Ω, and it is not identically zero. If S is a Kuramoto synchrony partition at a parameter value p^*, then $G^S_{a,c}(t;p^*) \equiv 0$ for all $t \geq 0$. In particular, $F^S_{a,c,t_0}(p^*) = G^S_{a,c}(t_0;p^*) = 0$. Hence, the set of parameter values for which this nontrivial incidence-count difference can be compatible with synchrony is contained in the zero set of the non-identically-zero real-analytic function F^S_{a,c,t_0}. Since the zero set of a nontrivial real-analytic function on a connected open domain has Lebesgue measure zero, this exceptional set has measure zero. Finally, the hypergraph is finite. Hence there are only finitely many candidate partitions, choices of representatives, receiving blocks, pairs of nodes, and possible incidence-count difference vectors. Taking the finite union of the corresponding exceptional parameter sets still gives a set of Lebesgue measure zero. Therefore, for almost every $p \in \Omega$, no two nodes in the same Kuramoto synchrony block can have a nonzero incidence-count difference toward the synchrony blocks. Equivalently, if $i, j \in S_a$, then $k^{(2)}_{i\beta} = k^{(2)}_{j\beta}$ for all β, and $k^{(3)}_{i\gamma\delta} = k^{(3)}_{j\gamma\delta}$ for all $\gamma \leq \delta$. Thus, every Kuramoto synchrony partition is equitable with respect to the interaction structure read by the dynamics. □

Theorem 2 (Conditional generic converse under separating signatures) *Consider a connected hypergraph $H = (N, E)$ with $\mathrm{rk}(H) \leq 3$ and the dynamics of Eq. (1) with identical natural frequencies $\omega_i = \omega_0$ and identical initial conditions $\theta_i(0) = \theta_0$ for all $i \in N$. Assume the separating interaction-signature condition stated above. Then, for almost every choice of parameters $p = (\alpha, \sigma_2, \sigma_3)$ with $\alpha \in (0, \pi/2)$ and $\sigma_2, \sigma_3 > 0$, the Kuramoto synchrony partition coincides with the fibration partition of H.*

Proof Let $S = \{S_1, \ldots, S_h\}$ be the Kuramoto synchrony partition and let $F = \{C_1, \ldots, C_q\}$ be the fibration partition. By Theorem III.7, for parameters outside an exceptional set of Lebesgue measure zero, any two nodes belonging to the same synchrony block have identical pairwise and three-body incidence counts toward the blocks of S. Hence S is an equitable partition for the incidence structure read by the dynamics. Since the fibration partition F is the coarsest equitable partition, any equitable partition S refines F; hence every block of S is contained in a block of F. Conversely, by Theorem 1, all nodes belonging to the same fibre have identical trajectories under the homogeneous Kuramoto–Sakaguchi dynamics. Hence, every fibre of F is contained in a synchrony block of S, so F refines S. The two refinements imply $S = F$. Therefore, under the stated assumptions and outside a Lebesgue-null exceptional subset of Ω, the Kuramoto synchrony partition coincides with the fibration partition. □

Remark 13 (Interpretation of assumptions in Theorem 2) Not all assumptions of Theorem 2 play the same conceptual role, and it is useful to distinguish between those that drive the exact synchrony mechanism and those that enter as model-specific or non-degeneracy requirements.

The core of the exact synchrony mechanism relies on homogeneity and nonzero frustration. Identical initial conditions and natural frequencies ensure that nodes with the same input structure receive identical dynamical contributions. The presence of a nonzero frustration parameter is also essential: it prevents the coupling from being non-invasive at the fully synchronous state and allows input-profile mismatches to affect the vector field. Requiring $\sigma_2, \sigma_3 \neq 0$ avoids degenerate cases in which an entire interaction order is inactive. For simplicity, we assume a common phase lag $\alpha \in (0, \pi/2)$ across interaction orders, but the mechanism only requires that the coupling contributions do not vanish at synchrony.

The converse direction also requires the separating interaction-signature condition stated before Theorem III.7. This condition is not a topological assumption on the hypergraph alone; it is a non-degeneracy requirement on the way the chosen admissible vector field reads the incidence structure. In the robust-synchrony theory for all admissible dynamics, the analogous separation is obtained by the freedom to choose coupling functions that distinguish unequal input profiles. In our fixed Kuramoto–Sakaguchi setting, the available interaction signatures are fixed, so we impose the corresponding independence condition explicitly. It excludes exact cancellations among distinct pairwise and three-body interaction contributions that would otherwise allow nodes with different incidence profiles to have identical trajectories on a positive-measure set of parameters.

The remaining assumptions are mainly related to modelling choices and analytical tractability. We restrict to $\mathrm{rk}(H) \leq 3$ because we focus on a specific higher-order Kuramoto model with pairwise and three-body interactions, derived in a principled way via phase reduction[24]. Similarly, the sinusoidal coupling is adopted to remain consistent with the classical Kuramoto framework, where it arises naturally. More general smooth coupling functions could be considered, provided analogous separation or non-degeneracy conditions are imposed to avoid cancellations between different interaction contributions.

In the numerical examples considered in this work, including the synthetic and real-world topologies, we did not observe non-fibration synchrony for generic choices of the parameters. This is consistent with the separating interaction-signature condition, although finite simulations do not prove that the condition holds for every hypergraph. A failure of the condition would require an exact analytic relation among the interaction signatures, rather than a small finite-time numerical coincidence.

Remark 14 The emergence of synchronization is governed not only by the presence of connections but also by the organization of interactions into fibres, subsets of nodes that share equivalent dynamical roles. These fibres are not intrinsic to the node set alone; they depend on how the system is represented. A hypergraph, its projection to a simple graph, or a multiedge graph can each induce different fibre structures as exemplified in Fig. 4. Under the homogeneity and non-degeneracy assumptions discussed above, the previous results show that this representation choice has a direct impact on which fibre-based groups are guaranteed, and generically expected, to synchronize. Thus, clusters predicted from an oversimplified representation need not remain coherent under the dynamics defined on the actual higher-order structure. This phenomenon is illustrated in Fig. 9, where the

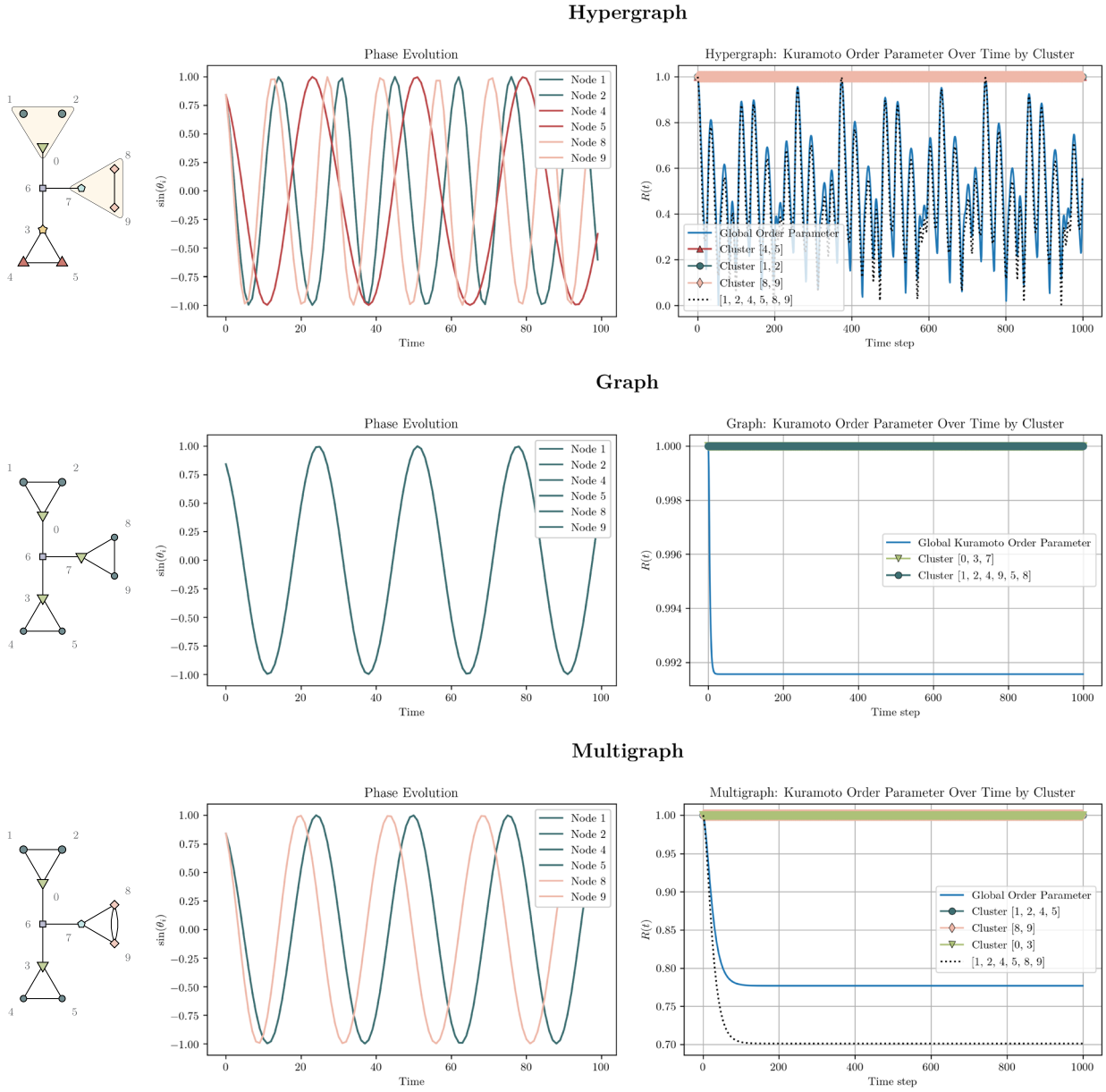


Fig. 9. Comparison of the dynamics of the higher-order Kuramoto model with frustration. The comparison is related to the example shown in Fig. 4 across three different representations reported on the left of the plots: the hypergraph (top row), its projection in a simple graph (middle row), and its projection in a graph with multiple edges (bottom row). The left plot shows the sine of the phase evolution over the first 100 time steps for the selected nodes [1, 2, 4, 5, 8, 9] that change fibre depending on the representation, colored according to the fibre they belong to. The right plot reports the local Kuramoto order parameter $R(t)$, measuring phase coherence within each fibre. Colored lines represent intra-fibre synchronization, and the blue thin line shows the global order parameter. For the hypergraph and the multi-order graph (lines 1 and 3), we also report with the dotted black line the measure of coherence computed for the subset of nodes [1, 2, 4, 5, 8, 9] (which is a fibre only for the simple graph) to illustrate different synchronization patterns across different representations. On the right, the intra-fibre local order parameters are completely overlapped as they are identically 1. This highlights how synchronization patterns can vary significantly depending on the chosen representation. The parameters for the dynamic Eq. (2) have initial condition and natural frequencies $(\theta_i, \omega_i) = (1, 0)$ for all nodes i, frustration parameter $\alpha = \pi/6$, and the strength parameters are $(\sigma_2, \sigma_3) = (0.2, 0.8)$.

same dynamical system is represented as a hypergraph (top row), a simple graph (middle), and a multiedge graph (bottom), with reference to Fig. 4. Although the parameters and initial conditions are identical, different sets of nodes synchronize in each case, corresponding to the different fibres. The set of represented nodes [1, 2, 4, 5, 8, 9] is split into three different fibres for the hypergraph, a unique fibre for the graph, and two fibres

for the multigraph. This structural condition coincides with the dynamical condition of cluster synchronization in the simulated example and is consistent with the conditional generic result above.

Trajectory-based extraction of empirical synchrony clusters

The theoretical analysis above identifies the fibre partition from the hypergraph topology. When the topology is known and reliable, Algorithm 1 is therefore the appropriate procedure to compute fibres directly from the incidence structure. The role of Algorithm 2 in this section is different and complementary: it operates on phase trajectories and extracts an empirical synchrony partition for a prescribed tolerance and observation window. In the numerical experiments of this paper, we use it as a diagnostic tool to compare the synchronized clusters observed in the dynamics with the fibre partition predicted from the topology. This trajectory-based viewpoint is also useful when one wants to observe how coherent clusters emerge from the dynamics without using structural information as input. In that case, Algorithm 2 can reveal groups of oscillators that synchronize empirically, and these groups can then be compared a posteriori with the fibre partition when the topology is available. Thus, the algorithm provides a way to inspect the dynamical manifestation of fibre clusters, but it should not be interpreted as a certified reconstruction of the fibration partition when the topology is unknown. The algorithm first restricts comparisons to nodes with the same degree sequence across hyperedge orders, following the necessary condition discussed in Theorem III.6. It then compares phase trajectories pairwise within each degree-based group. For pairs whose phases remain aligned at the sampled times, we compute the average local order parameter over time and identify values close to one as empirical pairwise synchrony. These pairwise relations are then merged by constructing an auxiliary undirected graph whose nodes are the Kuramoto oscillators and whose edges connect oscillator pairs detected as synchronized. The connected components of this auxiliary graph define the final empirical synchrony clusters. Trajectory-based clustering methods for Kuramoto-type dynamics have been studied in several contexts, including phase-coherence and robustness-based approaches[45,46]. Here, our use of such a procedure is diagnostic rather than inferential: under identical initial conditions, identical natural frequencies, and nonzero frustration, the simulations allow us to check whether the observed local synchronization patterns are consistent with the fibre partition computed from the hypergraph topology. The tolerance and observation window in Algorithm 2 are numerical parameters and do not enter the theoretical definition of the fibration partition; they only determine how empirical synchrony is detected from finite simulated or observed trajectories.

Input: Phase history matrix $\Theta \in \mathbb{R}^{T\times|N|}$, node groups $\{N_d\}_d$ by sequence of degree for all hyperedges orders, tolerance $\epsilon > 0$, number of time samples n.
Output: Set of synchronized clusters $C = \{C_1, \ldots, C_m\}$.
Step 1: Sample time points.
Randomly select n time indices $\{t_1, \ldots, t_n\}$ from $\{1, \ldots, T\}$.
Step 2: Iterate over degree-based node groups.
foreach *group of nodes* $V_d = N_d$ **do**
  Initialize a graph G_d with node set V_d.
  foreach *pair* $(i, j) \in V_d \times V_d$ **do**
    Extract trajectories $\theta_i(t)$ and $\theta_j(t)$ from Θ.
    if $|\theta_i(t_k) - \theta_j(t_k)| < \epsilon$ *for all* $k = 1, \ldots, n$ **then**
      Compute the average order parameter $\langle R_{ij}\rangle$ over all time.
      if $\langle R_{ij}\rangle > 1 - \epsilon$ **then**
        Add edge (i, j) to G_d.
      end
    end
  end
  Step 3: Extract synchronized clusters.
  Compute connected components $\{C_1^{(d)}, \ldots, C_{m_d}^{(d)}\}$ of G_d.
  foreach $C_\ell^{(d)}$ **do**
    Add $C_\ell^{(d)}$ to C.
  end
end
return C *(maximal synchronized clusters).*

Algorithm 2. Extracting synchronized clusters from HO Kuramoto with frustration dynamics.

Discussion

In this work, we have explored the relationship between local structural symmetries in undirected hypergraphs and the emergence of synchronization patterns in dynamical systems. We have deepened the understanding of fibration symmetry for complex systems with higher-order interactions, using the frustrated Kuramoto model as an example to study the dependence of topology on the emergence of cluster synchronization patterns.

However, our theoretical framework relies on a critical assumption that significantly limits its direct applicability to real-world processes: the requirement of identical initial conditions and natural frequencies across all nodes. This assumption, while mathematically necessary for our theoretical results, is unrealistic in natural systems. Real networks invariably exhibit heterogeneity in both initial states and intrinsic dynamics, making our exact synchrony conditions often unattainable. Despite these limitations, the conditional link between structural fibrations and homogeneous Kuramoto–Sakaguchi synchrony provides useful theoretical insight. In the exactly homogeneous setting, fibres define invariant synchrony subspaces, and under the separating interaction-signature condition, the trajectory-induced synchrony partition generically coincides with the fibration partition. This suggests possible algorithmic uses in clustering and community detection, provided the assumptions and the representation dependence of the result are kept explicit. The weak-heterogeneity tests reported in the Appendix indicate that the fibre partition can remain predictive under small static perturbations in the examples considered, but they should not be interpreted as a proof of transverse stability or as a stability diagram over parameter space. Future work could explore generalizations of the framework introduced here, including the development of enhanced algorithms beyond the greedy approaches presented here for topology modification problems. Such extensions help capture more nuanced forms of partial synchronization in systems where the exact fibre structure is absent. A complementary direction for future work is the analysis of the transverse stability of the synchronization patterns identified here, which governs their persistence under heterogeneity and noise and may require studying perturbations along possibly time-dependent cluster trajectories. Section A 3 collects exploratory heuristic procedures for fibre-preserving topology modifications. These procedures illustrate possible algorithmic uses of the incidence-fibration framework, but they are not intended as optimized or benchmarked methods. A systematic study of their optimality, scalability, and comparison with graph-based approaches is left for future work.

Methods

All simulations carried out throughout the paper, unless otherwise stated, solve the Cauchy problem by computing trajectories using the method (`LSODA`) from the Python library SciPy with step size 0.1. Synthetic hypergraphs are generated using `random hypergraph` from the `hypergraphx.generation.random` module from the Python library Hypergraphx by specifying the number of nodes and hyperedges of orders 2 and 3, then extracting the largest connected component.

Data availability

The datasets used in section Fibration symmetries for real-world datasets with HOI are from XGI dataset[40] and the MAG-10 dataset is from the preprocessed files in https://github.com/TheoryInPractice/overlapping-ecc/tree/master/data/MAG-10[41,42].

Code availability

The code used for the analysis in the paper is organized in https://github.com/margheritaberte/Fibration_symmetries_cluster_synchronization. The repository provides functions to compute the fibre partition (i.e., the coarsest equitable partition or minimal balanced coloring) for nodes of graphs, multigraphs, and hypergraphs, along with example notebooks that illustrate, visualize, and apply the algorithms discussed in the paper.

Received: 11 March 2026; Accepted: 7 July 2026
Published online: 16 July 2026

References

1. Brown, R. From groups to groupoids: a brief survey. *Bull. Lond. Math. Soc.* **19**, 113 (1987) (version consulted: April 2, 2012 with some corrections to previous latexed versions and some updates on the references).
2. Grothendieck, A. Technique de descente et théorèmes d'existence en géométrie algébrique. I. Généralités. Descente par morphismes fidèlement plats. In *Séminaire Bourbaki : Années 1958/59 - 1959/60, Exposés 169-204, Astérisque No. 5* 299–327 (Société mathématique de France, 1960).
3. Boldi, P. & Vigna, S. Fibrations of graphs. *Discrete Math.* **243**, 21 (2002).
4. Deville, L. & Lerman, E. Modular dynamical systems on networks. *J. Eur. Math. Soc.* **17**, 859 (2013).
5. Nijholt, E., Rink, B. & Sanders, J. Graph fibrations and symmetries of network dynamics. *J. Differ. Equ.* **261**, 4861 (2016).
6. Battiston, F. et al. Networks beyond pairwise interactions: structure and dynamics. *Phys. Rep.* **874**, 1 (2020),
7. Bick, C., Gross, E., Harrington, H. A. & Schaub, M. T. What are higher-order networks?. *SIAM Rev.* **65**, 686 (2023).
8. Leifer, I., Sánchez-Pérez, M., Ishida, C. & Makse, H. A. Predicting synchronized gene coexpression patterns from fibration symmetries in gene regulatory networks in bacteria. *BMC Bioinform.* **22**, 865 (2021).
9. Morone, F. & Makse, H. A. Symmetry group factorization reveals the structure-function relation in the neural connectome of Caenorhabditis elegans. *Nat. Commun.* **10**, 8596 (2019).
10. Golubitsky, M. & Stewart, I. Nonlinear dynamics of networks: the groupoid formalism. *Bull. Am. Math. Soc.* **43**, 305 (2006).
11. Makse, H. et al. Fibration symmetry-breaking supports functional transitions in a brain network engaged in language (2024).
12. Kamei, H. & Cock, P. J. A. Computation of balanced equivalence relations and their lattice for a coupled cell network. *SIAM J. Appl. Dyn. Syst.* **12**, 352 (2013).
13. Zhang, Y., Latora, V. & Motter, A. E. Unified treatment of synchronization patterns in generalized networks with higher-order, multilayer, and temporal interactions. *Commun. Phys.* **4**, 1 (2021).
14. Gambuzza, L. V. et al. Stability of synchronization in simplicial complexes. *Nat. Commun.* **12**, 1255 (2021).
15. Pecora, L. M., Sorrentino, F., Hagerstrom, A. M., Murphy, T. E.& Roy, R. Cluster synchronization and isolated desyn653 chronization in complex networks with symmetries. *Nat. Commun.* **5**, 5079 (2014).
16. Salova, A. & D'Souza, R. M. Cluster synchronization on hypergraphs. arXiv:2101.05464 [cond-mat, physics:nlin] (2022).
17. Nicosia, V., Valencia, M., Chavez, M., Díaz-Guilera, A. & Latora, V. Remote synchronization reveals network symmetries and functional modules. *Phys. Rev. Lett.* **110**, 174102 (2013).

18. Schaub, M. et al. Graph partitions and cluster syn658 chronization in networks of oscillators. *Chaos Interdiscipl. J. Nonlinear Sci.* **26**, 2563 (2016).
19. Kirkland, S. & Severini, S. Alpha-Kuramoto partitions from the frustrated Kuramoto model generalise equitable partitions. *Appl. Anal. Discrete Math.* **9** (2013).
20. Brede, M. & Kalloniatis, A. C. Frustration tuning and perfect phase synchronization in the kuramoto-sakaguchi model. *Phys. Rev. E* **93**, 062315 (2016).
21. Aguiar, M., Bick, C. & Dias, A. Network dynamics with higher-order interactions: coupled cell hypernetworks for identical cells and synchrony. *Nonlinearity* **36**, 4641 (2023).
22. Dutta, S. et al. Impact of phase lag on synchronization in frustrated kuramoto model with higher-order interactions. *Phys. Rev. E* **108**, 034208 (2023).
23. Moyal, B., Rajwani, P., Dutta, S. & Jalan, S. Rotating clusters in phase-lagged kuramoto oscillators with higher-order interactions. *Phys. Rev. E* **109**, 034211 (2024).
24. León, I., Muolo, R., Hata, S. & Nakao, H. Higher-order interactions induce anomalous transitions to synchrony. *Chaos Interdiscipl. J. Nonlinear Sci.* **34**, 013105 (2024).
25. Zhang, Y. et al. Deeper but smaller: Higher-order interactions increase linear stability but shrink basins. *Sci. Adv.* **10**, eado8049 (2024).
26. Zhang, Y., Lucas, M. & Battiston, F. Higher-order interactions shape collective dynamics differently in hypergraphs and simplicial complexes. *Nat. Commun.* **14**, 1605 (2023).
27. Salova, A. & D'Souza, R. M. Analyzing states beyond full synchronization on hypergraphs requires methods beyond projected networks. arXiv:2107.13712 [cond-mat, physics:nlin] (2021).
28. von der Gracht, S., Nijholt, E. & Rink, B. Hypernetworks: cluster synchronization is a higher-order effect. *SIAM J. Appl. Math.* **83**, 2329 (2023).
29. Makse, H. A., Boldi, P., Sorrentino, F. & Stewart, I. Symmetries of living systems: symmetry fibrations and synchronization in biological networks. arXiv:2502.18713 q-bio (2025).
30. Nijholt, E.& DeVille, L. Dynamical systems defined on simplicial complexes: symmetries, conjugacies, and invariant subspaces. *Chaos Interdiscipl. J. Nonlinear Sci.* **32**, 093131 (2022).
31. Kovalenko, K. et al. Equitability and explosive synchronisation in multiplex and higher-order networks. *Commun. Phys.* 10.1038/s42005-026-02543-5 (2026).
32. Boldi, P., Leifer, I. & Makse, H. A. Quasifibrations of graphs to find symmetries and reconstruct biological networks. *J. Stat. Mech. Theory Exp.* **2022**, 113401 (2022).
33. Gambuzza, L. V., Frasca, M., Sorrentino, F., Pecora, L. M. & Boccaletti, S. Controlling symmetries and clustered dynamics of complex networks. *IEEE Trans. Netw. Sci. Eng.* **8**, 282 (2021).
34. Leifer, I., Phillips, D., Sorrentino, F. & Makse, H. A. Symmetry-driven network reconstruction through pseudobalanced coloring optimization. *J. Stat. Mech. Theory Exp.* **2022**, 073403 (2022).
35. Leifer, I. *Symmetry-Inspired Analysis of Biological Networks, Dissertations, Theses, and Capstone Projects* (Springer, 2022).
36. Aldis, J. W. A polynomial time algorithm to determine maximal balanced equivalence relations. *Int. J. Bifurc. Chaos* **18**, 407 (2008).
37. Gallo, L. et al. Synchronization induced by directed higher696 order interactions. *Commun. Phys.* **5**, 1 (2022).
38. Boldi, P. The emergence of hypergraphs in complex system analysis. In *2023 IEEE 9th International Conference on Collaboration and Internet Computing (CIC)* 1–7 (2023).
39. Morone, F., Leifer, I. & Makse, H. A. Fibration symmetries uncover the building blocks of biological networks. *Proc. Natl. Acad. Sci.* **117**, 8306 (2020).
40. Landry, N. W. et al. XGI: a Python package for higher-order interaction networks. *J. Open Source Softw.* **8**, 5162 (2023).
41. I. Amburg, Veldt, N. & Benson, A. Clustering in graphs and hypergraphs with categorical edge labels. In *Proceedings of The Web Conference 2020 , WWW '20* 706–717 (Association for Computing Machinery, 2020).
42. Sinha, A. et al. An overview of Microsoft Academic Service (MAS) and applications. In *Proceedings of the 24th International Conference on World Wide Web, WWW '15 Companion* 243–246 (Association for Computing Machinery, 2015).
43. Muolo, R., Nakao, H. & Coraggio, M. When higher-order interactions enhance synchronization: the case of the Kuramoto model (2025). arXiv:2508.10992 nlin.
44. Goh, K.-I. et al. The human disease network. *Proc. Natl. Acad. Sci.* **104**, 8685 (2007).
45. Böhm, C., Plant, C., Shao, J. & Yang, Q. Clustering by synchronization, In *Proceedings of the 16th ACM SIGKDD International Conference on Knowledge Discovery and Data Mining, KDD '10* 583–592 (Association for Computing Machinery, 2010).
46. Shao, J., He, X., Yang, Q., Plant, C. & Böhm, C. Robust synchronization-based graph clustering. In *Advances in Knowledge Discovery and Data Mining* (eds. Pei, J. et al.) 249–260 (Springer, 2013).
47. Klickstein, I. & Sorrentino, F. *Generating Symmetric Graphs* 121102 (Woodbury, 2018).
48. Zou, M., Guo, W. & Chu, K.-F. Rewiring complex networks to achieve cluster synchronization using graph convolution networks with reinforcement learning. *IEEE Trans. Netw. Sci. Eng.* **11**, 4293 (2024).
49. Zou, T. et al. Control of chaotic synchronization in complex semiconductor lasers network: leveraging network structure symmetry. *Optics Express* **33**, 28243 (2025).
50. Iacopini, I., Petri, G., Barrat, A. & Latora, V. Simplicial models of social contagion. *Nat. Commun.* **10**, 2485 (2019).
51. Jost, J. & Mulas, R. Hypergraph Laplace operators for chemical reaction networks. *Adv. Math.* **351**, 870 (2019).
52. Alaygut, T. & Sefer, E. Hypergraph neural networks to predict stock movements by exploring higher-order relationships. In *Proceedings of the 6th ACM International Conference on AI in Finance, ICAIF '25* 700–708 (Association for Computing Machinery, 2025).

Acknowledgements

The authors acknowledge support from the project SoBigData.it "Strengthening the Italian RI for Social Mining and Big Data Analytics" - IR 000013 – CUP: B53C22001760006 funded by the European Union - Next Generation EU - National Recovery and Resilience Plan (Piano Nazionale di Ripresa e Resilienza, PNRR), PNRR Mission 4 Component 2 Investment 3.1.

Author contributions

T.G. and M.B. developed the concept of the study and contributed to the interpretation of results. M.B. implemented the simulations, performed the analyses, and drafted the manuscript. All authors reviewed and approved the final manuscript.

Funding

No funding.

Competing interests
The authors declare no competing interests.

Additional information
Supplementary Information The online version contains supplementary material available at https://doi.org/10.1038/s41598-026-61679-0.

Correspondence and requests for materials should be addressed to M.B.

Reprints and permissions information is available at www.nature.com/reprints.

Publisher's note Springer Nature remains neutral with regard to jurisdictional claims in published maps and institutional affiliations.

Open Access This article is licensed under a Creative Commons Attribution-NonCommercial-NoDerivatives 4.0 International License, which permits any non-commercial use, sharing, distribution and reproduction in any medium or format, as long as you give appropriate credit to the original author(s) and the source, provide a link to the Creative Commons licence, and indicate if you modified the licensed material. You do not have permission under this licence to share adapted material derived from this article or parts of it. The images or other third party material in this article are included in the article's Creative Commons licence, unless indicated otherwise in a credit line to the material. If material is not included in the article's Creative Commons licence and your intended use is not permitted by statutory regulation or exceeds the permitted use, you will need to obtain permission directly from the copyright holder. To view a copy of this licence, visit http://creativecommons.org/licenses/by-nc-nd/4.0/.

© The Author(s) 2026